



Infrared active vibrations in doped π -conjugated materials: the mechanism of activation of Raman modes

C Castiglioni and M Tommasini

Dipartimento di Chimica, Materiali e Ingegneria Chimica Giulio Natta, Politecnico di Milano, Milano, Italy.

We present here a theoretical investigation on the effect of doping polyacetylene with electron acceptor/donor species. Density Functional Theory (DFT) calculations, applied to selected molecular models, allow describing the response to the charge transfer, which highlights remarkable physical effects, like the relaxation of the molecular geometry and the softening of the vibrational frequencies. The analysis of the predicted spectroscopic observables gives insight about the origin of the strong doping-induced IR vibrational transitions, closely related to the major Raman bands of the undoped species. The analysis of the infrared intensities through local contributions based on electro-optical parameters reveals that intramolecular charge hopping is promoted by collective nuclear displacements along the Effective Conjugation Coordinate (ECC). © Anita Publications. All rights reserved.

Keywords: Polyacetylene, conducting polymers, doping, polaron, soliton, DFT simulations.

1 Introduction

Since the early synthesis of semiconducting polymers and oligomers, Raman and infrared (IR) spectroscopies have been extensively exploited for their structural assessment [1-3]. In the case of molecular materials characterized by delocalized π electrons, Raman spectroscopy allows to elucidate the fine-tuning of the electronic structure by means of changes of the molecular geometry and of inter-molecular interactions in crystalline or disordered phases [1-5]. For instance, the confinement of π electrons determined by the finite size of oligomers or by the presence of structural defects, shows its signature in Raman and IR spectra [4,5,6-10].

The dependence existing between the molecular structure and the electron density justifies the remarkable geometry relaxation associated with some electronic processes, like chemical doping and chemical functionalization, and it is unveiled by specific spectroscopic signatures. Notably, charge transfer upon doping allows the activation in the IR spectra of vibrational transitions that are strictly related to the lines which dominate the Raman spectra of the undoped (neutral) species. Such doping-induced IR bands often show remarkably high IR absorption intensity, with dipole strength comparable to that of electronic transitions [4,6,3,11]. In the literature, they were initially referred to as IR active vibrations or IR activated vibrations (IRAVs) [12,13], and more recently they have been renamed as Intense Vibrational Modes (IVMs) [14].

The phenomenon leading to the appearance of IRAVs is quite general, and the observation of IRAVs has been reported for a wide class of conducting polymers [1,2]. The early theoretical studies are focused on the prototypical case of polyacetylene (PA) [7,11-13,15-18]. The theories developed for the interpretation of the spectroscopic response of neutral and charged PA paved the way for the interpretation of the spectral features of more complex systems [2,3,8-10].

Corresponding author

e mail: chiara.castiglioni@polimi.it (C Castiglioni)

The rationalization of the appearance of IRAVs in doped and photo-excited PA was one of the main goals of the Amplitude Modes (AM) [15,16] and Effective Conjugation Coordinate (ECC) [7,18] theories. The fundamental credit of such theories was the identification of a peculiar collective nuclear displacement coordinate along which the coupling with the electronic structure is very sensitive. A displacement along this trajectory implies a collective and simultaneous stretching and shrinking of the adjacent CC bonds along the PA (or oligoene) chain, and it is named Bond-Length-Alternation (BLA) oscillation, or Effective Conjugation Coordinate (ECC) vibration [7,8,18]. The ECC coordinate corresponds to the dimerization parameter (u), which is central in the description of the π -electron-phonon interaction in PA [3,12]. Indeed, the ECC effectively describes how the π -electrons structure (i.e., the degree of delocalization of the π -electrons, or the π -conjugation length) affects the vibrational dynamics of PA and oligoenes. The ECC also plays a relevant role in phenomena like the polarisation of the electronic cloud driven by lattice deformation, and the lattice-assisted charge hopping. For oligoenes, the analytic expression of the ECC in terms of valence internal coordinates [19] is the following:

$$R_{ECC} = \frac{1}{\sqrt{N}} \sum_{j=1, N} (-1)^j R_j \quad (1)$$

Equation (1) holds for the general case of a linear oligoene with N CC bonds. R_j is the stretching coordinate of the j -th CC bond and the j index sequentially labels the CC bonds from one end to the other end of the chain. For introducing the ECC in PA, we take the limiting case of an oligoene of infinite length, i.e., we consider a 1D crystal whose translational unit cell contains one single and one double CC bond. According to [20], R_{ECC} is a phonon ($q = 0$, phonon wavevector) valence coordinate of A_g species defined as the out-of-phase stretching of the single (R_1) and of the double bond (R_2) belonging to the unit cell:

$$R_{ECC} = \frac{1}{\sqrt{2}} (R_1 - R_2) \quad (2)$$

For PA and its oligomers (i.e., the linear oligoenes) the two transitions which dominate the Raman spectrum are assigned to the ECC (or BLA) oscillation, which is coupled either in-phase or out-of-phase with a collective CH wagging vibration. Such two normal modes are often simply referred to as the ECC modes [18,7,8,10]. Even though the vibrational frequencies of the IRAV are rather far from those of the ECC Raman active transitions of neutral PA, both the AM and the ECC theory have identified the IRAV as the ECC modes of a charged (doped) chain. The remarkable frequency shift observed upon doping is ascribed to the sizeable softening of the force constant associated with the ECC coordinate, or, according to the AM theory, it is described by the renormalization of the vibrational modes upon charging. Moreover, the activation of the ECC modes in the IR spectrum (i.e., the onset of IRAVs) is justified by the symmetry breaking induced by the charge transfer. Differently from other theories [12,13,17] that describe the doping-induced defects as a finite size charged solitons embedded in a perfectly dimerized PA chain, the AM and the ECC theories describe the vibrational dynamics of PA, both in the pristine and in the doped form, by the model of an ideally infinite 1D crystal. The symmetry of neutral PA at the Γ point is C_{2h} , as it consists of a sequence of alternated quasi single and quasi double CC bonds (i.e., two CH groups per cell, with $BLA \neq 0$). In ECC and AM theories, the doping induced defect was described as a sequence of “equalized” ($BLA = 0$) CC bonds: the associated – ideally infinite – 1D crystal has a unit cell still containing two CH groups, with D_{2h} symmetry at the Γ point. The structure of the doped chain was inspired by the geometry predicted for charged solitons, e.g. computed by means of simple molecular models that exhibited a remarkable equalization of several CC bonds, leading to a delocalized charge defect [21,22]. Moreover, after charge transfer, all the CC bonds in the defected region become polarized and, in particular, the inversion centre of symmetry associated to each CC bond is lost. Both the ECC and the AM theory invoke a symmetry breaking driven by bonds polarization to justify the activation in the IR spectrum of the Raman active totally symmetric modes of the neutral chain. As it will be illustrated in the present work through Density Functional Theory (DFT) calculations, this phenomenon can be described more explicitly, by adopting a charge distribution pattern for the doped

undimerized 1D crystal based on molecular models. This results in a lowering of the symmetry of the soliton-like undimerized chain model at Γ point, from D_{2h} to C_{2v} . The ECC modes, that belong in neutral PA to A_g species (Raman active, IR inactive) are now classified as B_1 modes, thus they are IR *and* Raman active modes of the C_{2v} crystal.

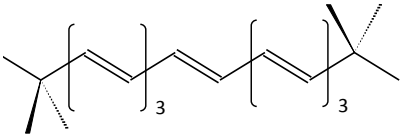
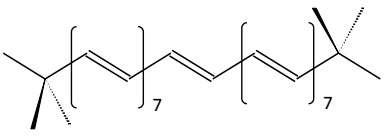
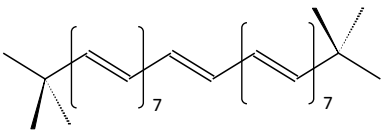
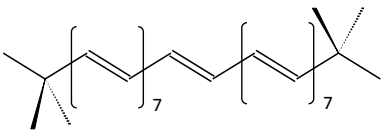
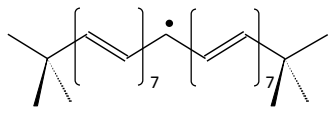
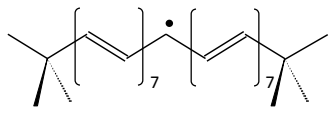
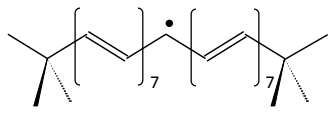
Both ECC and AM theory are successful, but they are empirical models. Furthermore, most of the theoretical studies on doped PA make use of semi-empirical Hamiltonians that were the most viable quantum chemical approach then available [3,12,13,17]. In more recent times, several DFT investigations of the vibrational properties of doped organic molecules have appeared in the literature [14, 23], driven by the renewed interest on highly conducting organic materials. In this framework, Anderson *et al* [14] presented an accurate experimental and theoretical study on the effect of doping on the copolymer PCPDTBT(poly[2,6-(4,4-bis(2-ethylhexyl)-4H-cyclopenta[2,1-b;3,4-b''dithiophene)-alt-4,7-(2,1,3-benzothiadiazole)]) and on the homo-polymer PCPDT (poly(cyclopentadithiophene)), highlighting some limitations of the AM and ECC models. The most important issue is the fact that the doped soliton (or polaron) is confined on several chemical units along the polymer backbone, which makes questionable the description of the dynamics of doped PA as it was an infinite 1D crystal.

Therefore, inspired by the analysis presented in [14,23], we have decided to discuss the IRAVs of PA, and their possible correlation with the Raman active ECC modes, by focusing on selected molecular models that are expected to closely approach the geometry and the electronic structure associated with localized charged solitons and polarons. The series of DFT calculations presented in this work aim at a thorough rationalization of the phenomena observed with IR and Raman spectroscopy, and allow to establish a link with the early theories of IRAVs.

2 Methods

We have carried out DFT calculations with the B3LYP/6-311G(d,p) method employing the Gaussian quantum chemistry package [24]. Full geometry optimization was carried out before the calculation of the normal modes and IR/Raman intensities. The computed values of the vibrational wavenumbers are reported without applying scaling factor, since the discussion focuses on the comparison among theoretical results.

Table 1. Sketch and description of the neutral and charged model molecules investigated. q is the total charge (electrons) and S the electronic spin number.

model	$q(e)$	S	$N(C)$	Symmetry	description	structure
a7	0	0	14	C_{2h}	neutral	
a15 (= a)	0	0	30	C_{2h}	neutral	
a+	1	1/2	30	C_{2h}	radical cation \rightarrow positive polaron	
a-	-1	1/2	30	C_{2h}	radical anion \rightarrow negative polaron	
b	0	1/2	29	C_{2v}	neutral radical \rightarrow neutral soliton	
b+	1	0	29	C_{2v}	cation \rightarrow positive soliton	
b-	-1	0	29	C_{2v}	anion \rightarrow negative soliton	

The all trans oligoenes investigated here (Table 1) are end capped by two tert-butyl groups, in analogy with the series of oligoenes analyzed in ref [5]. A neutral radical, i.e., an oligoene with an odd number of C atoms mimics the soliton structure. The cations and anions obtained from the corresponding neutral models mimic doped species obtained by withdrawal (or injection) of one electron charge: charged solitons (**b**+/-) or radical cations/anions (**a**+/-), i.e. polarons. For the sake of conciseness, we report and discuss in detail the results obtained for the positively charged species, whereas for the negatively charged species we will show only the simulated spectra. On the other hand, a thorough analysis of the structure and vibrational observables of **a**- and **b**- leads to the same conclusions as reported here for the positively charged species.

3 The Raman signature of the electron-phonon coupling: ECC theory and conjugation length

The ECC coordinate is very sensitive to the delocalization of π electrons along the molecular skeleton: for this reason, the Raman spectrum gives straightforward evidence about the extent or confinement of the distribution of π -electrons. When considering a series of oligoenes, irrespective to the end groups, a remarkable [5,10] shift of the peak position of the strong Raman features (ECC modes), is always observed for increasing chain length [4,6,8,10]. The decrease of the force constant associated with the ECC (F_{ECC}) not only explains the dramatic frequency shift of the IRAV compared with the corresponding ECC modes of neutral PA, but also the decrease of the frequency of the ECC modes while increasing the oligoene length. The longer the conjugation length, the lower the force constant associated with ECC and the vibrational frequencies. Furthermore, parallel to F_{ECC} , the equilibrium structure of oligoenes of increasing length shows a progressively more pronounced equalization of the CC bonds.

As initial step, we test our quantum chemical models of the neutral species considering the properties discussed above. Figure 1 reports the simulated Raman spectrum of two neutral oligoenes with 7 and 15 CC double bonds. As expected, passing from 7 to 15 double bonds, the two most intense Raman bands remarkably shift ($\Delta\nu_1 = 64 \text{ cm}^{-1}$; $\Delta\nu_2 = 74 \text{ cm}^{-1}$). Moreover, as reported in Table 2, the Raman activities of the main bands increase by about 2 orders of magnitude passing from **a7** to **a15**.

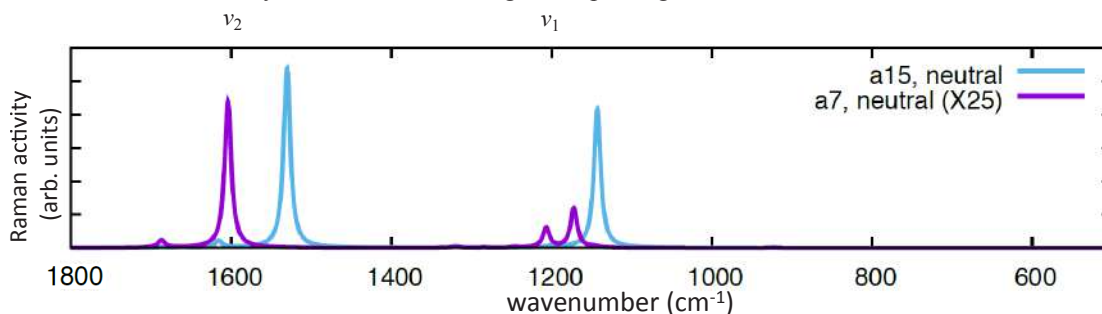


Fig 1. Raman spectra simulated by DFT of two oligoenes with 7 (**a7**) and 15 (**a15**) double CC bonds (see Table 1 for details).

The changes of the relevant structural parameter (BLA) for increasing chain length are also reported in Table 2. The BLA values have been obtained by averaging the difference of the equilibrium bond lengths of pairs of adjacent CC bonds along the chain ($\langle \text{BLA} \rangle$), or by taking the difference of the bond lengths of the central pair of CC bonds ($[\text{BLA}^{\text{CB}}]$). As expected, both $\langle \text{BLA} \rangle$ and $[\text{BLA}^{\text{CB}}]$ decrease passing from **a7** to **a15**.

The representation of the vibrational eigenvectors of **a7** and **a15** reported in Fig 2 clearly show that ν_1 and ν_2 are ECC modes: both of them largely involve a collective stretching and shrinking of the adjacent CC bonds. However, for both molecules (notably **a7**) in the ν_2 mode the contribution of the stretching of

quasi-double CC bonds is larger than that of quasi-single CC bonds, at difference of ν_1 that shows a larger contribution from single CC bond stretching. Moreover, the coupling of ECC with the CH in-plane bending vibrations has a different relative phase: ν_1 can be described as the oscillation along ($R_{\text{ECC}} + \text{CH bending}$) whereas ν_2 is described as ($-R_{\text{ECC}} + \text{CH bending}$).

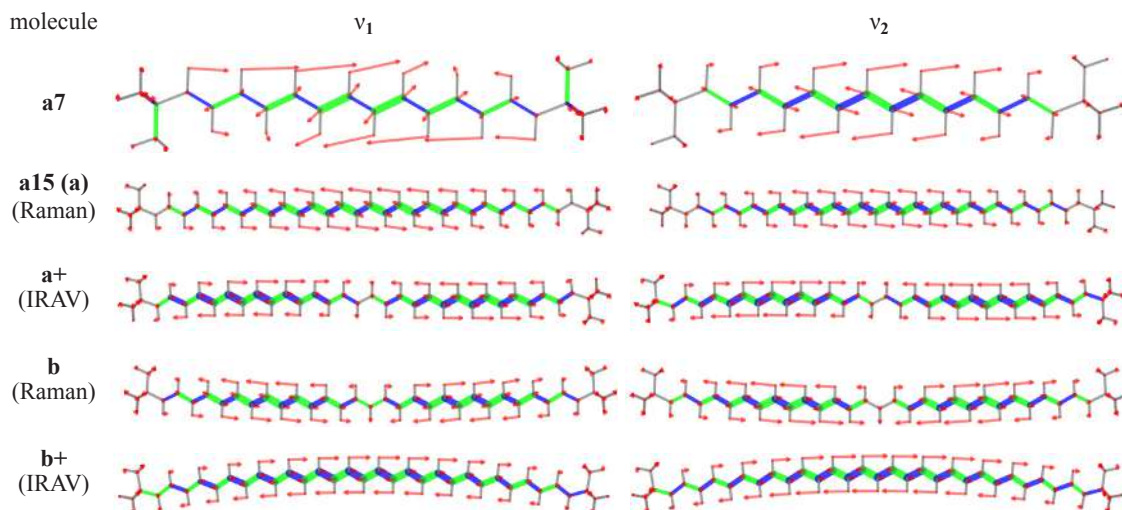


Fig 2. Representation of the vibrational normal modes associated with the very strong Raman or IR (IRAV) ECC modes of selected model molecules illustrated in Table 1. Red arrows represent displacement vectors; CC bonds are represented as green (blue) lines of different thicknesses according to their relative stretching (shrinking). The associated intensities are highlighted in bold in Table 2.

Table 2. Raman and IR observables (wavenumber, Raman activity, IR intensity) of the ECC modes computed by DFT for selected oligoenes described in Table 1. In the second column the equilibrium values of the BLA parameters are reported. Wavenumbers labelled with (*) correspond to ECC-like modes showing a displacement pattern with a central node. Very strong IRAV or Raman intensities are highlighted in boldface.

Molecule	$\langle \text{BLA} \rangle$ [BLA^{CB}] (\AA)	ν_1 (cm^{-1})	ν_2 (cm^{-1})	I_1 ($\text{\AA}^4 \text{amu}^{-1}$)	I_2 ($\text{\AA}^4 \text{amu}^{-1}$)	I_1 (km mol^{-1})	I_2 (km mol^{-1})
a7	0.0836 [0.0712]	1207	1604	3.6×10^4	2.7×10^5	-	-
a (a15)	0.0703 [0.0602]	1143 1171*	1530 1578*	6.5×10^6 -	8.5×10^6 -	- 1	- 206
a+ radical cation	0.0306 [0.0022]	1087 1102*	1472 1475*	1.1×10^6 -	5.9×10^5 -	- 2.8×10^4	- 2.1×10^4
b radical	0.0453 [0.0062]	730 1086*	1399 1472*	4.2×10^4 2.4×10^6	5.2×10^3 1.5×10^6	102 0	57 0
b+ cation	0.0362 [0.0041]	1089 1179*	1471 1551*	5.6×10^3 5.9×10^5	2.6×10^3 2.1×10^6	7.3×10^4 11	4.6×10^4 35

The histogram of Fig 3 allows rationalizing the occurrence of very large Raman intensities for the ECC modes. This is done through the evaluation of local parameters, namely the polarizability derivatives

with respect to CC stretching coordinates. Indeed, the derivative of the molecular polarizability along the ECC modes is mainly due to the large contributions arising from the CC stretching coordinates [10], and the following equation holds:

$$\frac{\partial \alpha^{uv}}{\partial Q_k} = \sum_t \frac{\partial \alpha^{uv}}{\partial r_t} L_{tk} \cong \sum_i \frac{\partial \alpha^{uv}}{\partial R_i} L_{ik} \quad (3)$$

According to [19], Q_k is the k -th normal coordinate, $\{r_i\}$ is the set of the internal valence coordinates, L_{tk} is the matrix element of the vibrational eigenvector, $\{R_i\}$ is the sub-set of the CC stretching internal coordinates.

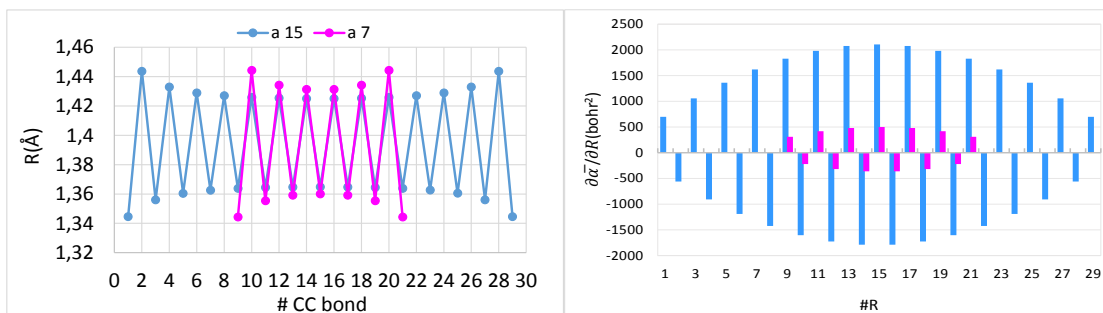


Fig 3. Left panel: equilibrium CC bond distances computed by DFT for two oligoenes with 7 (**a7**) and 15 (**a15**) double CC bonds. Right panel: contributions to the polarizability derivatives arising from individual CC bonds along the oligoene chain, namely $\partial \bar{\alpha} / \partial R_i$ parameters.

Since in oligoenes, the tensors $\partial \alpha / \partial R_i$ have one dominant diagonal element in the direction of the main molecular axis [10], we can discuss the behaviour of $\partial \alpha / \partial Q_k$ by simply considering their trace, indicated as $\partial \bar{\alpha} / \partial R_i$. These values are reported in Fig 3. The adjacent single and double CC bonds stretching show values of $\partial \bar{\alpha} / \partial R_i$ with opposite sign. According to Eq (3), the contributions from the individual CC bonds to $\partial \alpha / \partial Q_k$ sum up, which implies large Raman intensities for the ECC modes. This is due to the fact that also L_{ik} have opposite signs when the i label indicates a single or a double bond, since in ECC modes the single and double bond stretch out-of-phase, according to Eq (1).

4 IRAV

We consider now the models designed for the description of charged defects that approach the structure of a charged polaron (**a15+**) and a charged soliton (**b+**). The oligoene **a15** (hereafter referred simply as case **a**) describes the “reference” neutral species for the singly charged polaron, while the radical **b** is the neutral reference for **b+**.

Figure 4 illustrates the equilibrium CC bond lengths along the backbone of the three models **a**, **a+**, **b+**. The charged species show a remarkable relaxation of the equilibrium structure toward a more equalized geometry, especially in the inner region. This structure rearrangement is quantified in Table 2 by the decrease of the $\langle \text{BLA} \rangle$ and $[\text{BLA}_{\text{CB}}]$ values for **a+** and **b+**.

Remarkably, the point group symmetry of these molecular structures changes in pairs: the neutral soliton (**b**) and the charged solitons (**b+/b-**) belong to the C_{2v} point group, whereas **a** and the **a+(a-)** polarons belong to the C_{2h} point group. The presence of the inversion symmetry in the C_{2h} group implies a perfect mutual exclusion of IR and Raman transitions for **a**, **a+**, and **a-**. This promptly reveals that by charging a molecule with C_{2h} symmetry one cannot admit the activation in the IR of Raman active vibrations. On the other hand, the in-plane modes of the C_{2v} structures can have simultaneous IR and Raman activity.

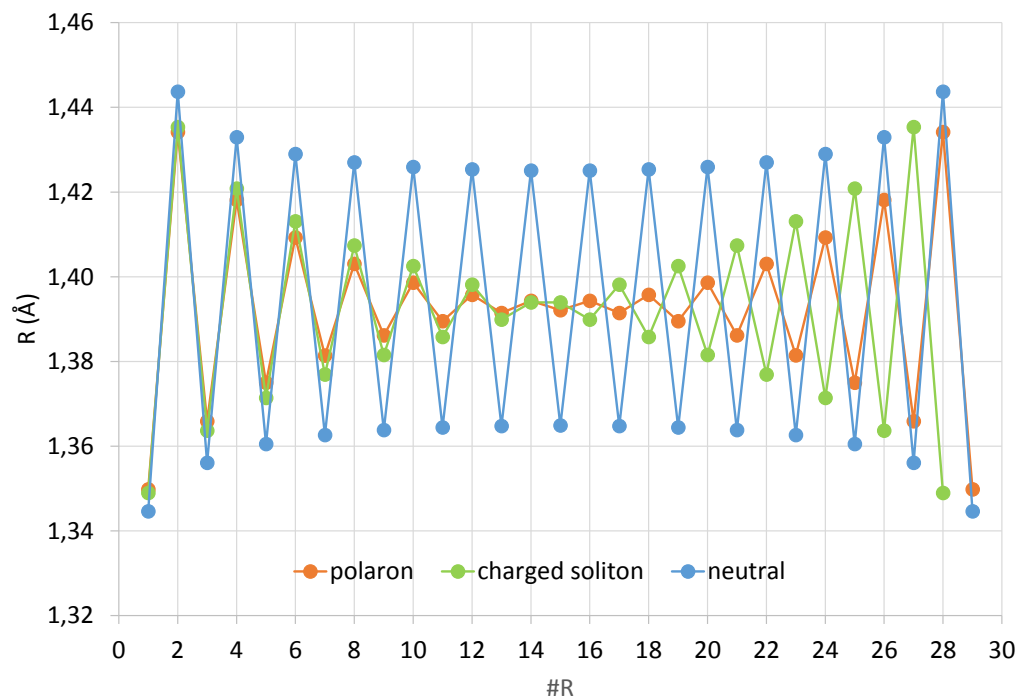


Fig 4. Equilibrium CC bond distances of the models **a** (neutral), **a+** (polaron) and **b+** (charged soliton) as computed by DFT.

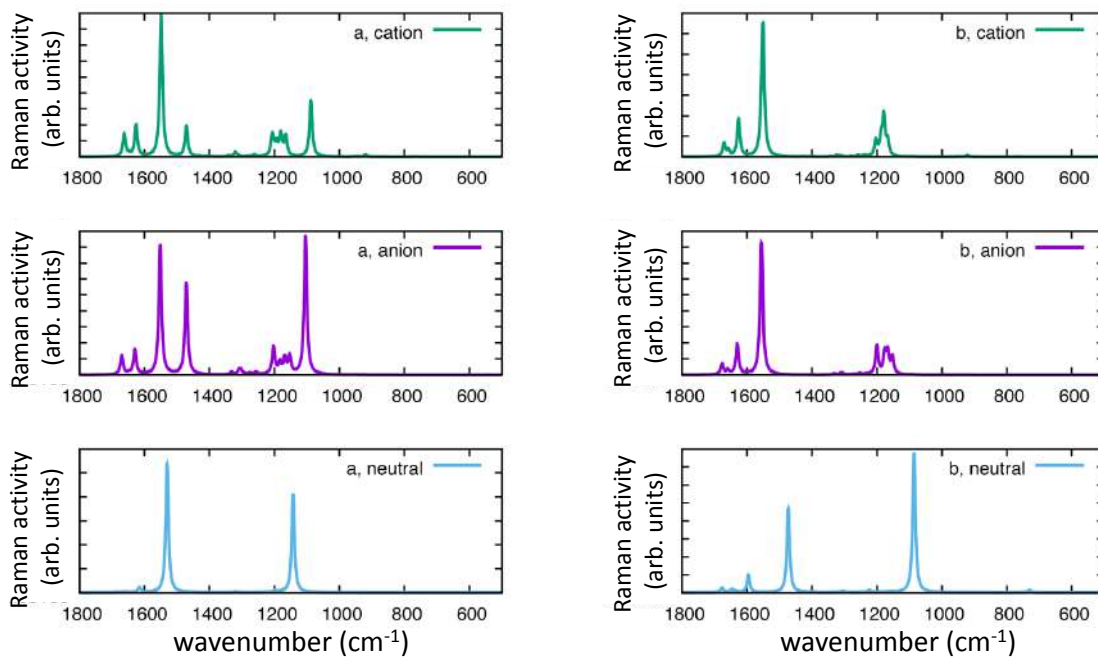


Fig 5. Raman spectra simulated by DFT of the model molecules that describe the neutral and charged (doped) species.

For these models, the simulated Raman spectra reported in Fig 5 show that:

- the Raman spectra of the neutral species (**a**, **b**) are very selective, and they display two very strong lines assigned to ν_1 and ν_2 ECC modes (see Fig 2 for the illustration of the associated nuclear displacements);
- the Raman spectra of the charged species are richer of bands that show non-negligible intensities;
- by passing from **a** to **a+** one observes a remarkable weakening of the Raman intensity of the ECC modes, especially for the ν_2 line that decreases by one order of magnitude (see Table 2).

Interestingly, in the neutral soliton (**b**), the two very strong Raman lines (ν_1 , ν_2) correspond to ECC-like vibrations of A_1 symmetry species whose displacements patterns (Fig 2) are similar to those of the neutral oligoene (**a**), but show a node, in correspondence of the central C atom. Remarkably, in the neutral soliton one observes the inversion of the single-double CC bond alternation pattern from the left- to the right-hand side of the central C atom (Fig 4), thus the A_1 displacement pattern (ECC with a central node) is the true BLA oscillation in this case. It is also worth mentioning that the frequencies of the ECC modes of the neutral soliton model (**b**) are remarkably lower than those of the neutral oligoene (**a**).

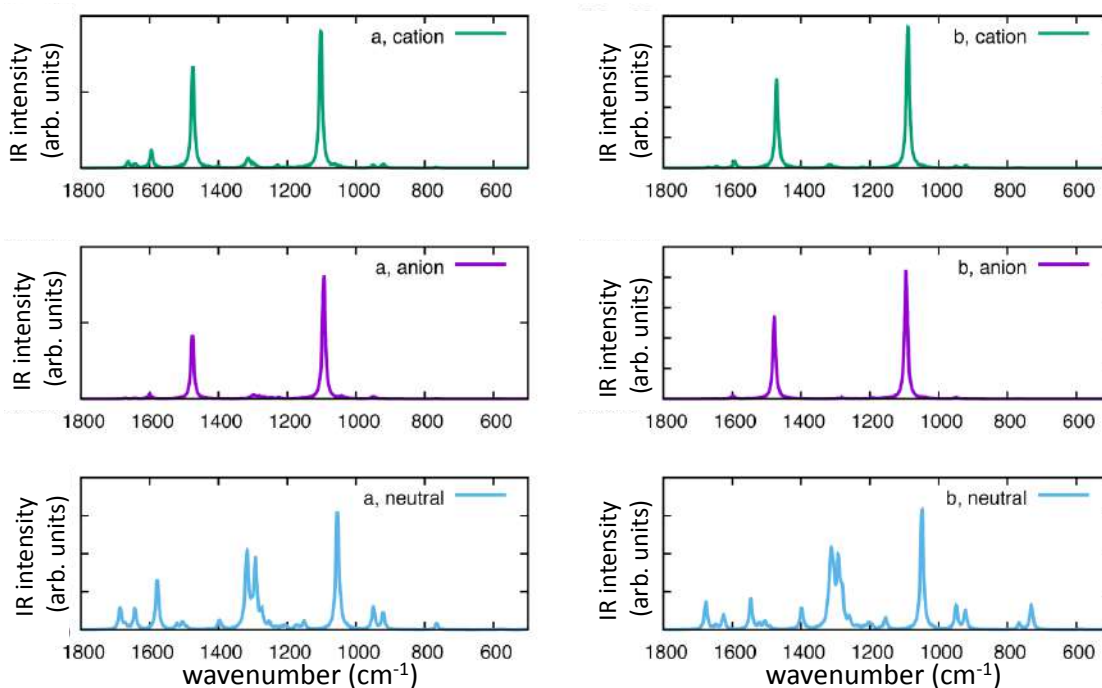


Fig 6. IR spectra simulated by DFT of the model molecules that describe the neutral and charged (doped) species.

Figure 6 reports the IR spectra of the models of the neutral oligoene, the neutral soliton, and of the charged species. In this case, we obtain very strong and selective IR spectra for all the charged species, with two ECC bands (IRAVs) that dominate the spectra. Very importantly, the neutral species display ordinary IR spectra that show several transitions with comparable IR intensity.

By looking at the IR intensities reported in Table 2, one realizes that this feature is caused by the fact that in the IR spectra of **a** and **b** the transitions associated to ν_1 and ν_2 are weak, with intensities that are about two orders of magnitude lower than the two IRAVs which arise upon charging. In other words, also the charged species have a manifold of IR active modes of comparable strength, but their intensities are vanishingly small when compared with the two exceptionally strong IRAVs. This result is very important,

since it proves that the quantum chemical models adopted here can describe the onset of the IRAVs that is observed upon doping PA. In addition, the appearance of very strong IR bands, overwhelming any other IR transition, our quantum chemical models nicely reproduce the second remarkable experimental evidence, namely the decrease of the wavenumber of the IRAVs with respect to the Raman active ECC modes of the neutral (pristine) species.

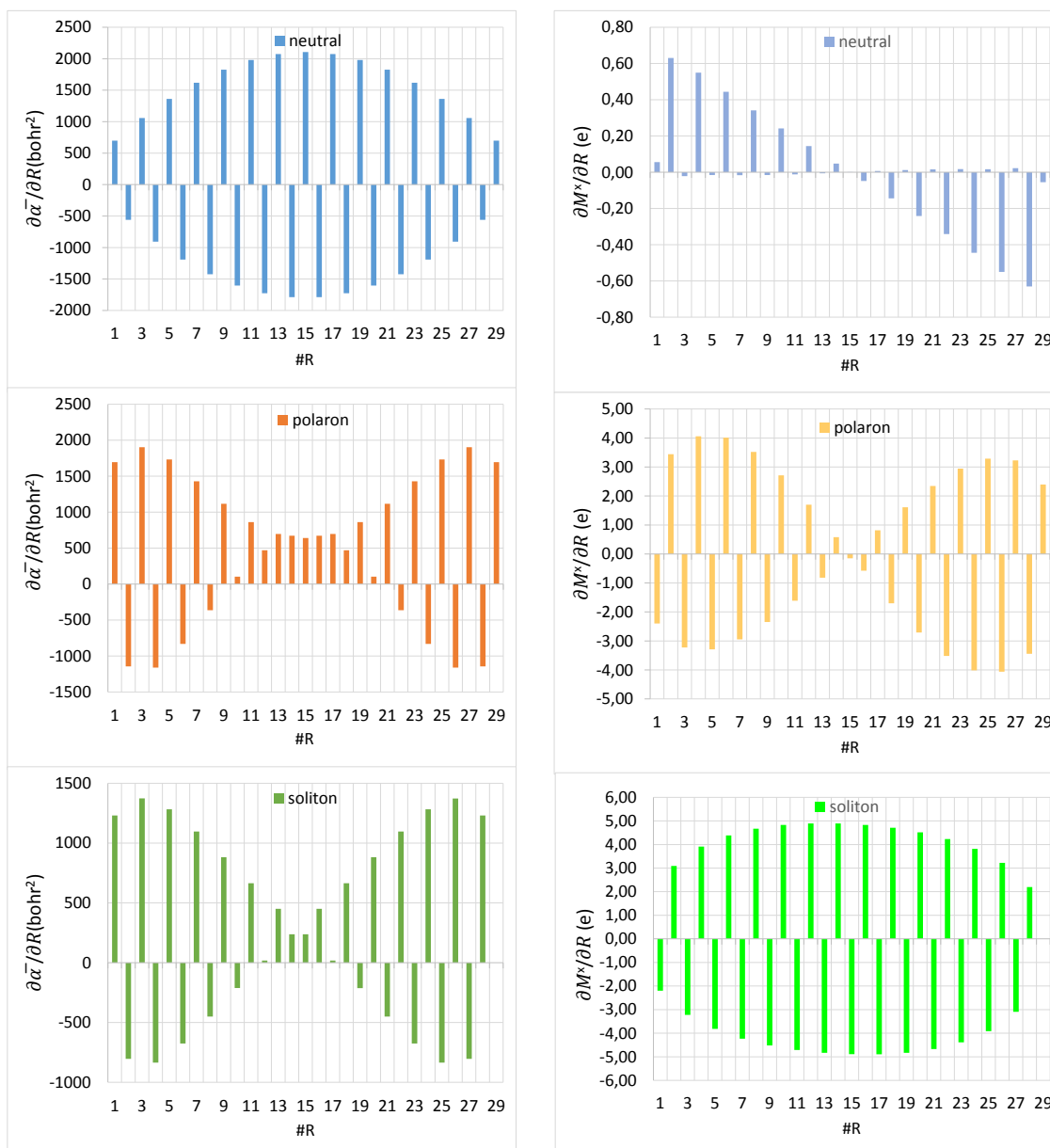


Fig 7. *Left panels:* individual contributions to the polarizability change $\partial\bar{\alpha}/\partial R_i$ with the stretching of the CC bonds along the chain. *Right panels:* individual contributions to the dipole moment change $M^x/\partial R_i$ with the stretching of the CC bonds along the chain. From the top to the bottom: model molecules **a** (neutral), **a+** (polaron), **b+** (soliton).

Also in the case of the charged species Eqs (1) and (3) can rationalize the trends observed for the Raman intensities of the ECC modes. The left panels of Fig 7 show $\partial\bar{\alpha}/\partial R_i$ parameters that occur upon charging. The most remarkable effect in the central section of the chain of **a+** and **b+** is the loss of the pattern typical of the neutral oligoene (with opposite signs for adjacent CC bonds). This pattern change is observed in **a+** and **b+** in correspondence of equilibrium values of BLA that approach 0. This implies that for the ECC modes of the charged species the central CC bonds provide a vanishing contribution to the total polarizability derivative, $\partial\alpha/\partial Q_k$ because of the quasi-perfect cancellation of the similar contributions from adjacent stretching coordinates, when they oscillate out-of-phase.

A similar analysis is presented in the right panel of Fig 7 for the individual IR local parameters $\partial M^x/\partial R_i$, namely the molecular dipole derivatives with respect to individual CC stretching coordinates. Similar to Eq (3), Eq (4) provides the expression of $\partial M^x/\partial Q_k$, which leads to the IR intensities of the ECC modes:

$$\frac{\partial M^x}{\partial Q_k} = \sum_t \frac{\partial M^x}{\partial r_t} L_{tk} \cong \sum_i \frac{\partial M^x}{\partial R_i} L_{ik} \quad (4)$$

For the neutral species, the pattern of the $\partial M^x/\partial R_i$ parameters (Fig 7) tells us that the ECC modes are silent in the IR: the contributions arising from the right-hand side of the central CC bond cancel those coming from the left-hand side, which is expected based on symmetry selection rules. Moreover, $\partial M^x/\partial R_i$ parameters are small, which is also expected because the CC bonds are apolar in neutral oligoenes.

The situation is completely different for the **a+** and the **b+** cases. In both cases, the stretching of adjacent CC gives $\partial M^x/\partial R_i$ parameters with opposite sign. Interestingly, while crossing the centre of the **a+** molecule, one observes the inversion of the $\partial M^x/\partial R_i$ pattern: in the left side $\partial M^x/\partial R_i$ is negative for odd i values and positive for even i values, while in the right side $\partial M^x/\partial R_i$ is positive for odd i and positive for even i . This inversion of the $\partial M^x/\partial R_i$ pattern does not happen in **b+**. Hence, by simply considering the $\partial M^x/\partial R_i$ patterns and Eq (4), we can predict strong IR activity for the B_1 ECC mode of **b+** (without nodes) and for the B_u ECC mode of **a+** (with a central node).

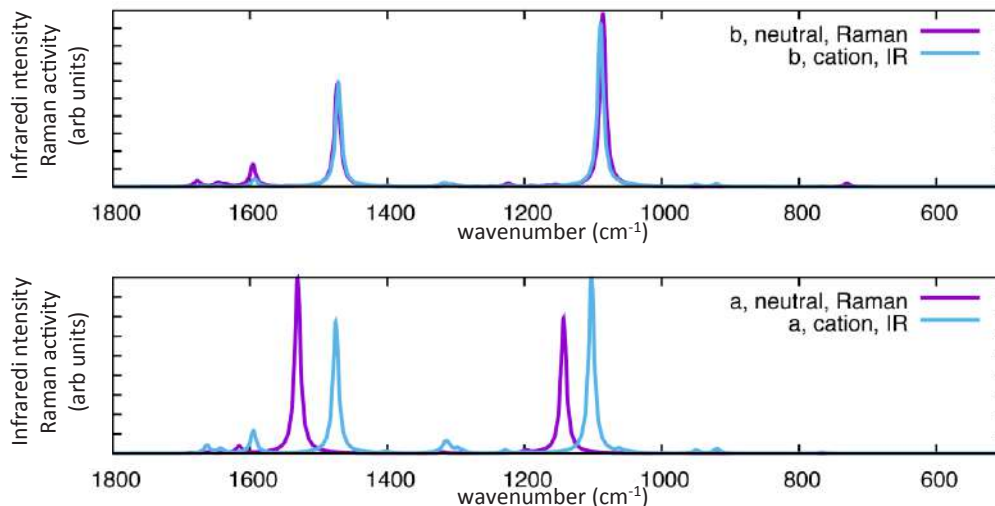


Fig 8. Comparison between the Raman and IR spectra simulated by DFT of the neutral and of the corresponding positively charged model: top **b/b+**; bottom: **a/a+**.

Figure 8 summarizes the Raman/IR response of the **a**, **a+** and **b**, **b+** models. It is apparent that the neutral species show intense and selective Raman spectra, whereas the charged species have a very strong

and selective IR spectra, dominated by IRAV. Interestingly, both the neutral (**b**) and charged (**b+**) species (mimicking the soliton like defect) and the **a+** species (mimicking a charged polaron) show lower frequencies than the neutral oligoene (**a**), which indicates that the decrease of the ECC wavenumber is highly correlated with the relaxation toward an equalized structure (small BLA). Moreover, a smaller BLA value is also the evidence of a more effective π -electron conjugation.

5 IR activation: interpretation by means of local IR parameters

We have analysed further the positive soliton model (**b+**), to better highlight the mechanism at the basis of the activation of IRAVs. According to the Equilibrium Charges - Charge Fluxes (ECCF) model, it is possible to identify two contributions to the dipole moment derivatives $\partial M/\partial Q_k$, namely: (i) the effect of the displacement of atoms carrying fixed partial charges (equilibrium charges), (ii) the charge fluxes associated with atomic vibrations (i.e., the change of the atomic charges induced by nuclear displacements). It is shown in Ref [7] that the intensities of the IRAVs, caused by the very large dipole derivatives associated with the ECC modes, cannot be accounted for by a model with just fixed equilibrium charges. This holds even in presence of the non-negligible fractional charges on the C atoms that result from the excess charge transferred by the doping process. The charge distribution of the doping-induced charge defect has been firstly described several years ago in the pioneering work by Brédas *et al* [21,22], through the inspection of the Mulliken charges of a soliton-like model oligoene. Features that are similar to those reported in [21,22] are reproduced by our calculations on **b+**, when looking at the distribution of the equilibrium excess charge that is present at each C site (Fig 9). Each CH group is considered as a whole, by summing the equilibrium charges on the C and H atoms of each CH group. We have computed the atomic charges according to the ECCF model, starting from the Atomic Polar Tensors computed by DFT, and applying the procedure illustrated in [25,26]. Figure 9 shows that the fractional positive charges are localized on the CH sites with odd index, while the even index CH sites carry smaller and negative charges. The right-hand side panel of Fig 9 shows the plot of the change of the CH charges caused by a geometry displacement, $\Delta Q_1 = 0.1 \text{ \AA amu}^{1/2}$, along the normal coordinate associated with the strongest IR active ECC mode (ν_1). The plot shows that, for a positive displacement along the ECC mode, the charges on the left-hand side of the central C atom increase (become more positive), whereas the charges on the right-hand side decrease (becomes more negative). This results in a net displacement from right to left of the hole injected by doping.

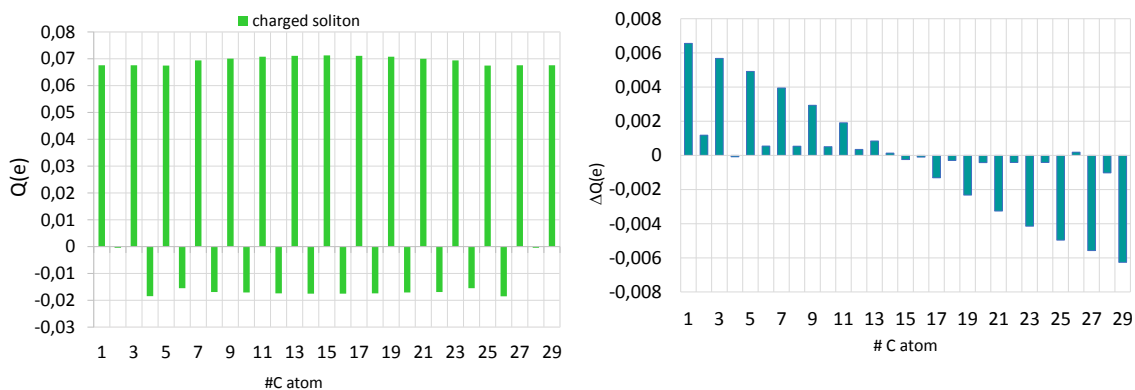


Fig 9. Localized charges and charges fluctuation calculated for the model of positively charged soliton (**b+**). *Left panel*: excess charge localized at carbon atoms sites after charging the radical molecule **b** (soliton). Localized charges are obtained according to refs [25,26], see text. *Right panel*: changes of the local charges on C atoms, after atoms displacement along the ECC mode Q_1 ($\Delta Q_1 = 0.1 \text{ \AA amu}^{1/2}$).

This outcome is very impressive because it directly correlates the nuclear dynamics described by the ECC with the transport of the hole, which turns out to be assisted by such peculiar vibrational trajectory: it is the evidence, at the molecular level, of the strong electron-phonon coupling that influences the charge transport phenomena in polyconjugated materials.

6 Conclusions

The first goal of this study was to revise the early interpretation of the doping-induced IRAV features observed in polyconjugated systems, notably PA. A theoretical analysis through DFT calculations carried out on selected oligoenes in neutral and charged states, allowed reproducing the relevant spectroscopic features experimentally observed. Moreover, this investigation confirmed that peculiar trajectories in the vibrational space (i.e., the ECC modes) are responsible both of the selective and strong Raman spectra of the neutral species, and of the appearance of IRAV bands upon charging.

The subtle question addressed in ref [14] whether the vibrational modes responsible for the IRAVs of doped species are the same as the strongly Raman active ones of their neutral counterparts, finds here an answer coming from the detailed vibrational assignment and the comparison of the different models considered.

Based on the symmetry point group of each model molecule, we conclude that:

- (i) the charging (by ionization) of finite size neutral molecules (**a**, **b**) does not cause a change of the symmetry point group;
- (ii) **a**, **a+** and **a-** belong to the C_{2h} group, which implies that Raman active modes are not IR active (mutual exclusion);
- (iii) **b**, **b+** and **b-**, because of their C_{2v} symmetry, show modes that are simultaneously IR and Raman active.

The analysis of the vibrational eigenvectors associated to the most prominent Raman and IR bands shows that:

- (iv) the v_1 and v_2 modes that dominate the Raman spectrum of **a** and the IR spectrum of **b+** (**b-**) possess a large contribution from the collective vibrational ECC coordinate, described by the alternate stretching/shrinking of adjacent CC bonds;
- (v) the v_1 and v_2 modes which dominate the Raman spectrum of the radical species **b** are assigned to a collective ECC vibration that shows a node at the centre of the molecule and belongs to A_1 species. The same displacement pattern (ECC with a central node) describes the IRAV of the charged polaron models **a+** and **a-**.

According to points (i-v), we agree with ref. [14]: the analysis of finite size models allow stating that the collective vibrational displacements associated to the strong Raman features **are not the same** which describe the IRAV bands. However, one finds a quasi-perfect correspondence of the nuclear displacement patterns if one compares the pairs (**a**, **b+**) and (**b**, **a+**). Furthermore, the comparison between the neutral C_{2h} molecule **a** with the charged C_{2v} model **b+** suggests that a symmetry change is needed for the activation in the IR of the Raman modes. Remarkably, this symmetry change corresponds to the same required for passing from an infinite neutral and dimerized PA chain (1D crystal, C_{2h} symmetry factor group at Γ) to a 1D crystal with fully equalized, and polarized CC bonds, mimicking the doped PA chain. Indeed, for an asymmetric distribution of the excess charge, like the one illustrated in Fig 9, the doped 1D chain loses the inversion centre, which results in a C_{2v} structure that allows the activation in the IR of the Raman active A_g phonons of the neutral chain. In particular, the out-of-phase CC stretching corresponding to the ECC vibrational displacement (Eq 1), which characterizes the two strongly Raman active ECC phonons of the neutral chain, becomes a B_1 symmetry coordinate of the charged chain, whose associated phonons may display a large IR intensity (see Section 5).

Our finite size models also provide a molecular description of the frequency softening (or renormalization) caused by doping, as predicted by AM and ECC theories. Moreover, the detailed inspection of the vibrational eigenvectors of the ECC modes for **a** and **b**⁺ species clearly proves their very close similarity (Section 3).

In summary, based on the analogy between the ideal infinite models and the molecular models investigated here, we finally understand why AM theory and ECC theory - in their early formulation applied to the 1D crystal - had such a remarkable interpretative power.

The most important issue of these pioneering approaches was the conceptual incompatibility between a lattice defect, involving a finite number of CC bonds, and the translational symmetry assumed for modelling doped PA as a 1D crystal. In this respect, it is important to recall that lattice defects in PA do involve several CC bonds, so that collective normal modes of a finite chain, can be described quite well by selected phonons of the parent 1D crystal [20]. It is also remarkable that the AM theory tried to manage this issue while introducing the concept of a pinning potential to which a real doping-induced defect is subjected, because of the presence of a counterion, or by conjugation defects along the chain.

On the other hand, the possibility to perform high-level first principle calculations now provides us with a detailed description of a variety of charge defects, accompanied by a geometry relaxation confined in a finite-size molecular domain. For instance, C_{2h} defects, mimicking charged polarons, can be hardly described with an infinite chain model but are nicely modelled by charging a long C_{2h} polyene. Such models tell us that a mere activation of the ECC Raman modes in the IR cannot be always invoked, while ECC-like vibrations (ECC with a node) can carry very strong IR activity without the need of any “symmetry breaking”.

The analysis of our models confirms the strong coupling among π -electrons and vibrational modes. This is proven by the geometry relaxation along ECC, namely the change of the equilibrium BLA value that occurs upon charging and by the remarkable softening predicted for the ECC modes.

Further evidence of the electron-phonon coupling through ECC vibrations is the finding that the strong infrared intensity of IRAV is associated to the hole hopping across the charge defect. This indicates that doping induced intra-chain charge mobility could benefit of lattice geometry fluctuations occurring along the ECC direction, i.e., associated to BLA oscillation.

Acknowledgements

Chiara Castiglioni is deeply grateful to her mentors, Mariangela Gussoni and Giuseppe Zerbi, and to her friend J Teodomiro López Navarrete, with whom she shared the intellectual challenge of developing the ECC theory in its first formulation. Matteo Tommasini is also very grateful for their enthusiastic input and guidance in applying quantum chemical methods to the vibrational spectroscopy of π -conjugated materials.

References

1. Skotheim T A, (ed.). Handbook of Conducting Polymers, (Dekker, New York), 1986.
2. Brédas J L, Silbey R, (eds.). Conjugated Polymers: The Novel Science and Technology of Highly Conducting and Nonlinear Optically Active Materials, (Springer Netherlands), 1991.
3. Heeger A J, Kivelson S, Schrieffer J R, Su W P, Solitons in Conducting Polymers, *Rev Mod Phys*, 60 (1988)781–850.
4. Harada I, Furukawa Y, Tasumi M, Shirakawa H, Ikeda S, Spectroscopic studies on doped polyacetylene and β -carotene, *J Chem Phys*, 73(1980)4746–4757.
5. Schaffer, H E, Chance, R R, Silbey, R J, Knoll, K, Schrock, R R, Conjugation length dependence of Raman scattering in a series of linear polyenes: Implications for polyacetylene, *J. Chem. Phys.*, 94 (1991) 4161-4170.
6. Piaggio P, Dellepiane G, Piseri L, Tubino R, Taliani C, Polarized infrared spectra of highly oriented polyacetylenes, *Solid State Commun*, 50(1984)947–956.

7. Gussoni M, Castiglioni C, Zerbi G, Vibrational spectroscopy of polyconjugated materials: polyacetylene and polyenes. In Clark R J J, Hester R E (eds.), *Spectroscopy of advanced materials*, (Wiley, New York), 1991, Ch 5, pp 251-353.
8. Castiglioni C, Del Zoppo M, Zerbi G, Vibrational Raman Spectroscopy of Polyconjugated Organic Oligomers and Polymers, *J Raman Spectrosc*, 24(1993)485–494.
9. Zerbi G, Gussoni M, Castiglioni C, Vibrational spectroscopy of polyconjugated aromatic materials with electrical non-linear properties. In Brédas J L, Silbey R, (eds), *Conjugated Polymers: The Novel Science and Technology of Highly Conducting and Nonlinear Optically Active Materials*, (Springer Netherlands), 1991, p 435.
10. Castiglioni C, Tommasini M, Zerbi G, Raman Spectroscopy of Polyconjugated Molecules and Materials: Confinement Effect in One and Two Dimensions, *Philos Trans R Soc A*, 362(2004)2425–2459.
11. Vardeny Z V, Ehrenfreund E, Brafman O, Horovitz B, Fujimoto H, Tamoka J, Tareka M, Detection of soliton shape modes in polyacetylene, *Phys Rev Lett*, 57(1986)2995–2998.
12. Mele E J, Rice M J, Vibrational excitations of charged solitons in polyacetylene, *Phys Rev Lett*, 45(1980)926–929.
13. Etemad S, Pron A, Heeger A J, MacDiarmid A G, Mele E J, Rice M J, Infrared-active vibrational modes of charged solitons in $(\text{CH})_x$ and $(\text{CD})_x$, *Phys Rev B*, 23(1981)5137–5141.
14. Anderson M, Ramanan C, Fontanesi C, Frick A, Surana S, Cheyng D, Furno M, Keller T, Allard S, Scherf U, Beljonne D, D’Avino G, von Hauff E, Da Como E, Displacement of polarons by vibrational modes in doped conjugated polymers, *Phys Rev Materials*, 1(2017)055604; doi.org/10.1103/PhysRevMaterials.1.055604.
15. Ehrenfreund E, Vardeny Z, Brafman O, Horovitz B, Amplitude and phase modes in trans polyacetylene resonant Raman- scattering and induced infrared activity, *Phys Rev B*, 36(1987)1535–1553.
16. Vardeny Z, Ehrenfreund E, Brafman O, Horovitz B, Resonant Raman Scattering from Amplitude Modes in trans- $(\text{CH})_x$ and $(\text{CD})_x$, *Phys Rev Lett*, 51(1983)2326-2329.
17. Painelli A, Girlando A, Del Freo L, Soos Z G, Infrared intensity and local vibrations of charged solitons, *Phys Rev B*, 56(1997)15100–15108.
18. Castiglioni C, Navarrete J T L, Zerbi G, Gussoni M, A simple interpretation of the vibrational spectra of undoped, doped and photoexcited polyacetylene: Amplitude mode theory in the GF formalism, *Solid State Commun*, 65 (1988)625-630.
19. Wilson E B, Decius J C, Cross P C, *Molecular Vibrations: The Theory of Infrared and Raman Vibrational Spectra*, (McGraw-Hill, New York), 1955.
20. Zbinden R, *Infrared Spectroscopy of High Polymers*. (Academic Press, New York), 1964
21. Chance R, Boudreaux D S, Brédas, J L, Silbey R. Solitons, Polarons and Bipolarons in Conjugated Polymers. In Skotheim T A, (ed.). *Handbook of Conducting Polymers* (Dekker, New York), 1986, p 825.
22. Chance R, Boudreaux D S, Brédas J L, Silbey R, Neutral and charged soliton defects in polyacetylene, *Phys Rev B*, 27(1983)1440–1442.
23. Denti I, Cimò S, Brambilla L, Milani A, Bertarelli C, Tommasini M, Castiglioni C, Polaron Confinement in *n*-Doped P(NDI2OD-T2) Unveiled by Vibrational Spectroscopy, *Chem Mater*, 31(2019)6726–6739.
24. Gaussian 09, Revision D.01, Frisch M J, Trucks G W, Schlegel H B, Scuseria G E, Robb M A, Cheeseman J R, Scalmani G, Barone V, Petersson G A, Nakatsuji H, Li X, Caricato M, Marenich A, Bloino J, Janesko B G, Gomperts R, Mennucci B, Hratchian H P, Ortiz J V, Izmaylov A F, Sonnenberg J L, Williams-Young D, Ding F, Lipparini F, Egidi F, Goings J, Peng B, Petrone A, Henderson T, Ranasinghe D, Zakrzewski V G, Gao J, Rega N, Zheng G, Liang W, Hada M, Ehara M, Toyota K, Fukuda R, Hasegawa J, Ishida M, Nakajima T, Honda Y, Kitao O, Nakai H, Vreven T, Throssell K, Montgomery J A (Jr), Peralta J E, Ogliaro F, Bearpark M, Heyd J J, Brothers E, Kudin K N, Staroverov V N, Keith T, Kobayashi R, Normand J, Raghavachari K, Rendell A, Burant J C, Iyengar S S, Tomasi J, Cossi M, Millam J M, Klene M, Adamo C, Cammi R, Ochterski J W, Martin R L, Morokuma K, Farkas O, Foresman J B, Fox D J, Gaussian, Inc., Wallingford CT, 2016.
25. Dinur U, Charge Flux and Electrostatic Forces in Planar Molecules, *J Chem Phys*, 95(1991)6201–62011.

26. Galimberti D, Milani A, Castiglioni C, [Infrared intensities and charge mobility in hydrogen bonded complexes, *J Chem Phys*, 139\(2013\)074304](#); doi.org/10.1063/1.4818416.

[Received: 27.11.2021; accepted: 24.12.2021]



Chiara Castiglioni

Since 2010, she is Full Professor in Materials Science and Technology, at the Department of Chemistry, Materials and Chemical Engineering (DCMIC) Giulio Natta of Politecnico di Milano, Italy and leads the Laboratory of Molecular Spectroscopy at FuNMat Lab (Organic Functional and Nanostructured Materials Laboratory) of CMIC.

She was Coordinator of the Ph D Program in Materials Engineering, PoliMi (2010-2019); International Advisory Board of the Congress on Synthetic Metals ICSM2014, ICSM2016, ICSM2018 (since 2011); and Member of Editorial Board of Journal of Raman Spectroscopy (Wiley) since 2011.

Her research activity started with the thesis in Physics on the analysis of experimental infrared absorption intensities for the characterization of the charge distribution in molecules and with a Ph D dissertation on vibrational dynamics and spectroscopy of polyacetylene. She applied IR and Raman spectroscopy, in conjunction with Quantum Chemical modelling, to the study of organic polyconjugated molecules and polymers, polycyclic aromatic molecules, graphenes and carbon nanotubes. The focus was on the effects of π -electron delocalization vs. confinement related to molecular size and/or defects, on the study of charge carriers and transport properties in chemically or electrochemically doped materials. She contributed to the development of the Effective Conjugation Coordinate Theory and to a model for the determination of molecular hyperpolarizabilities from vibrational intensities. Her recent interests concern the study of nanostructured carbon materials (graphene nanoparticles, polyynes and molecular graphenes), applications of the microspatially offset Raman spectroscopy (micro-SORS) to cultural heritage, novel piezoelectric materials.

She is author of about 260 scientific papers on peer reviewed International Journals, contributions to books/handbooks; ORCID: <https://orcid.org/0000-0002-6945-9157>.



Matteo Tommasini

Since 2014, he is Associate Professor in Materials Science and Technology at the Dept. of Chemistry, Materials and Chemical Engineering (Politecnico di Milano). Since 2019 he is member of the Scientific Committee of the Italian group of vibrational spectroscopy (VISPEC). In 2021, with the patronage of the Società Italiana di Ottica e Fotonica (SIOF) he has coordinated a series of VISPEC online seminars, with several invited speakers, to foster scientific exchange and promote the diverse applications of vibrational spectroscopy and related techniques.

Since his thesis in Nuclear Engineering (1998) and the following Ph D in Materials Engineering (2002), under the guidance of Prof Chiara Castiglioni and Prof Giuseppe Zerbi, he has been investigating the spectroscopic behavior

of materials. In the following years, he further developed his skills in the field of vibrational and electronic techniques (resonant/non-resonant Raman scattering, IR absorption, and UV-Visible absorption). He adopted both experimental and theoretical techniques (quantum chemistry and development of physical models). The materials that he investigated include nanostructured carbon materials, graphene molecules, organic functional materials, and polymers. In 2013 he began a research activity on the detection of drugs by Surface Enhanced Raman Spectroscopy (SERS) for clinical applications. He is author of about 160 scientific papers published in peer reviewed international journals; ORCID: <https://orcid.org/0000-0002-7917-426X>.